Use of a pulsed laser to study properties of CdZnTe pixel detectors

Aleksey E. Bolotnikov, Steven E. Boggs, Walter R. Cook, Fiona A. Harrison, Steven M. Schindler

Aleksey E. Bolotnikov, Steven E. Boggs, Walter R. Cook, Fiona A. Harrison, Steven M. Schindler, "Use of a pulsed laser to study properties of CdZnTe pixel detectors," Proc. SPIE 3769, Penetrating Radiation Systems and Applications, (1 October 1999); doi: 10.1117/12.363691

SPIE.

Event: SPIE's International Symposium on Optical Science, Engineering, and Instrumentation, 1999, Denver, CO, United States

Use of a pulsed laser to study properties of CdZnTe pixel detectors

A. E. Bolotnikov, S. E. Boggs, W. R. Cook, F. A. Harrison, S. M. Schindler

Space Radiation Laboratory, California Institute of Technology
Pasadena, CA 91125

ABSTRACT

We have investigated the utility of employing a short (<4 ns) pulsed laser with wavelength tunable between 600-950 nm as a tool for studying and characterizing CdZnTe detectors. By using a single mode optical fiber and simple optics, we can focus the beam to a spot size of less than 10 μm and generate the number of the excess carriers equivalent to a several MeV gamma-ray either at the surface or deep inside the sample. The advantages of this technique over use of a collimated X-ray or alpha particle source are strong induced signal, precise pointing, and triggering capability. As examples of using this technique, we present the results of measurements of the drift velocity, electron lifetime, and electric field line distribution inside CZT pixel detectors.

Keywords: CdZnTe detector characterization

1. INTRODUCTION

The development of focal plane CdZnTe (CZT) pixel detectors for the High Energy Focusing Telescope (HEFT)[1] requires the development of test systems for selecting and characterizing detector-grade CZT, studying detector performance, and optimizing contact geometry and electronics. Test systems require highly collimated sources of radiation (alpha particles or X-ray sources, X-ray tubes, laser beams) to generate excess carriers in the bulk or on the surface of CZT detectors. Previously we described our X-ray test system[2]; here we report on results of tests performed with a pulsed laser system.

Using a laser beam to generate excess carriers in semiconductors is a convenient technique to investigate the properties of semiconductors and semiconductor detectors, Si[3], and CZT[4,5] in particular. In the case of CZT detectors, this technique becomes especially useful as a probe for selecting detector-grade material.

A short (~ 1 ns) pulsed laser beam focused to a spot size of less than 10 μm allows us to simulate the ionization effects which would be produced by ionizing particles, e.g. alpha particles or X-rays, inside CZT detectors. In many cases this technique has a number of advantages over the use of ionizing particle sources. For example, with the pulsed laser it is possible to create a large number of localized carriers, which induce strong and easily detectable signals on detector electrodes. By choosing the wavelength of the light longer than 800 nm, one can imitate particle tracks and create ionization deep inside a sample[6]. The beam spot can be visually seen and its location precisely measured with a microscope. In addition, the laser provides a fast coincidence trigger with each event, which permits accurate event counting and timing studies of the CZT signals.

In this work we used a pulsed laser to generate signals in CZT pixel detectors which were fabricated as part of our HEFT development program. We studied the charge collecting efficiency, electric field distribution, and contact geometry. In addition, the pulse shape analysis of the signals generated by the laser allowed us to measure basic material properties of CZT such as carrier lifetime and drift velocity.

2. EXPERIMENTAL SETUP

The beam from the tunable nitrogen laser (Laser Science, Inc., model VSL-337ND) was delivered through a single-mode 4.2 μm, 2 m long optical fiber and focusing optics to the CZT sample, which was mounted on X-Y motion stage controlled by a PC. The chosen approach for the light-beam delivery allowed us to eliminate electromagnetic noise produced by the laser and to make a more flexible and easily adjustable system. The focusing optics was a set of airspaced doublets comprised of two GRADIUM[7] lenses, which provided a < 10 μm diameter spot with very sharp edges. The duration of the laser pulses (FWHM) was about 4 ns, with an adjustable frequency up to 50 Hz. The laser provides a coincident trigger signal, delayed by 25 ns with 5 ns jitter with respect to the rising edge of the optical output. This trigger allows us to determine the start of signals with an accuracy of ~5 ns. Although the amplitude stability of the laser is only about 5%, the

Part of the SPIE Conference on Penetrating Radiation Systems and Applications
Denver, Colorado • July 1999 SPIE Vol. 3769 • 0277-786X/99/$10.00

main factor that determines the fluctuations in the number of excited carriers produced, especially when the surface of the CZT sample is coated with metal contacts, is the variation in surface reflectivity. In addition, scratches and other defects on the surface significantly reduce the signal through scattering. For studying the pixel response, this drawback can be eliminated by using the cathode signal to normalize the corresponding pixel signal for each event. It is important to mention that the beam should be slightly off normal angle with respect to the sample surface in order to avoid beam scattering back onto the detector.

To demonstrate the capability of the system, we tested several pixel and monolithic detectors available in our laboratory. The pixel detectors used in these measurements were originally fabricated to investigate the influence of contact geometry on the charge collection efficiency and energy resolution, and are described in Ref. 2. These detectors were 10x10x2 mm thick, high resistivity substrates bought from two different vendors. Each detector has different groups of gold contacts on one side and a monolithic contact (cathode) on the other. Each contact group consisted of a 4x4 array of identical contacts evenly spaced on a 500 μm pitch grid and enclosed within a guard ring. The contact sizes vary from group to group over the range 100 to 450 μm. The detectors were coupled to fan-outs using indium bump-bonding technology. The output pads of the fan-outs were wirebonded to the input pads of printed circuit boards containing hybrid charge-sensitive preamplifiers with a 20 ns risetime and 100 μs decaytime constants.

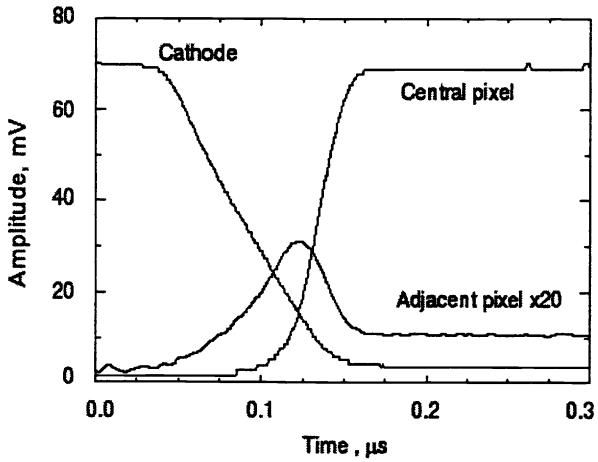

Figure 1. Shapes of the signals read out from the cathode, central, and adjacent contacts. Note that the signal from the adjacent contact is multiplied by a factor of 20, the bias is -200 V.

For the measurements discussed here, we selected a 650 nm wave length to generate excess carriers at the surface of the CZT samples. Signals from the cathode and three selected pixels were read out with a Tektronix TDS 540 digital oscilloscope controlled by a PC via GPIB. For each trigger event, waveforms (or measured amplitudes) were stored in each of the oscilloscope's four channels. The applied negative bias voltage was varied between 25 and 700 V.

3. RESULTS AND DISCUSSION

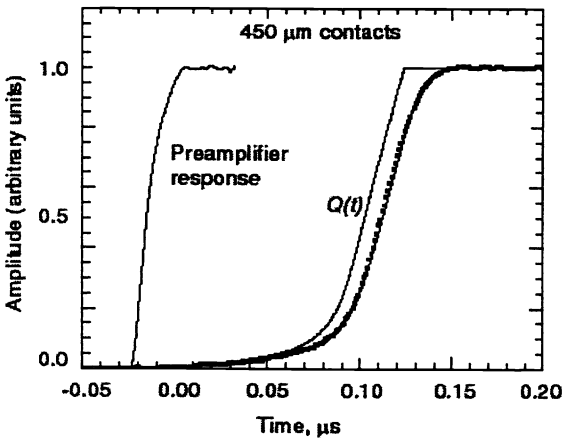

Figure 2. Time dependence of the induced charge on the pixel contact $Q(t)$. The preamplifier response indicates the beginning of the pulses. The black squares represent the measured shape of the pixel pulse.

A great deal of information can be gained from pulse shape analysis of the measured signals. The penetration depth of the laser beam (650 nm) was estimated be less than 1 μm, thus we could assume that all carriers were produced near the surface (on the cathode side in these measurements) and only drifting electrons contributed to the signals. In order to simplify analysis the laser beam was normally focused opposite the center of the selected pixel contact (we call it the central contact) to ensure that all generated electrons would be collected on a single pixel, i.e. no charge sharing among adjacent pixels. The signals induced on the central and surrounding contacts, and on the cathode as well, were measured for different detector biases. As an example, the measured signals from the cathode, central, and adjacent contacts are shown in Fig. 1. The cathode signal has a nearly linear rise, corresponding to the simple parallel plate geometry. The collected charge signal from the central pixel is "delayed" and has a much shorter rise time due to the shielding effect of other pixel contacts. The slowly rising portion of the induced signal on adjacent pixels is similar to that of the central pixel. However, the signal rapidly drops as carriers approach the

central pixel. If there were no electron trapping in the CZT the induced signal on adjacent pixels would drop back to zero.

3.1. Pulse shape of the signals

Considering a CZT detector as a simple parallel plate ionization chamber with homogeneous field distribution, one can expect, in the first approximation, a linearly rising shape for the cathode signals. The electron losses due to trapping, however, causes a slight bending of the cathode signals, while the response of the preamplifier smoothes the top of the pulse.

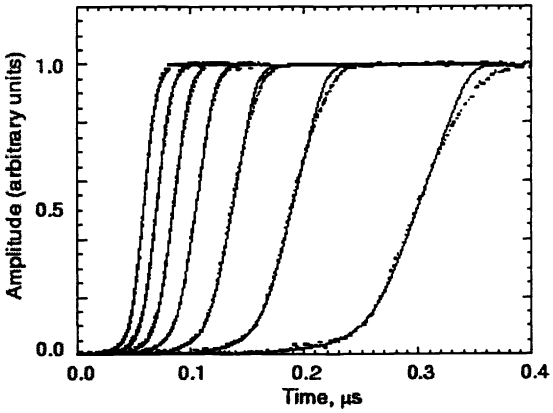

Figure 3. Results of the fitting procedure applied to the signals read out from a selected pixel to evaluate the electric field dependence of the electron drift velocity. The negative bias was varied between 50 and 600 V.

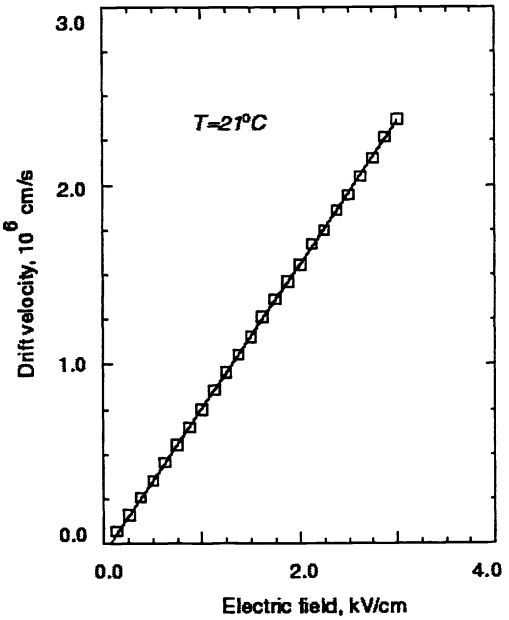

Figure 4. Dependence of the electron drift velocity on the electric field strength evaluated from TCT measurements. Note that the size of squares does not represent the statistical errors, which were very small.

Due to the shielding effect, the pixel signals are expected to increase slowly at first, with a sharp rise at the end of the drift near the contact. The typical pixel pulse shape is shown in Fig. 2. Four processes were considered to affect the pulse shapes: dependence of the induced charge on the electron cloud location, i.e. the weighting field function; response of the preamplifier; electron diffusion; and trapping. Because a typical pulse duration was about 0.1-0.2 μs, the electron de-trapping process, which takes place on a 10 μs scale, could be neglected. In particular, this effect could be seen on a 10 μs scale as a slowly rising signal component.

Numerical modeling showed that for bias voltages above 100 V, the pixel pulse shapes are not affected significantly by the electron diffusion and trapping (trapping affects the amplitude of the signal). Thus, the function to describe the measured shapes of the pixel pulses can be obtained as a result of convolution of the time dependence of the induced charge on the pixel $Q(t)$, and the response function of the preamplifier $R(t)$. If assume that the time dependence of the induced charge on the pixel $Q(t)$ can be described as a function of t/t_{drift}, i.e. $Q(t)=Q(t/t_{drift})$, where t_{drift} is the total drift time, then one can use a single function $Q(t/t_{drift})$ to fit all the pixel pulse shapes measured at different biases. For instance, the latter condition is obvious if the electric field is uniform inside the CZT.

The response function of the preamplifier was measured by applying a fast step-like pulse (<3 ns rise time) through a calibrating capacitor to the inputs of the preamplifiers. The rise time of the preamplifiers was found to be less than 20 ns. The time dependence of the induced charge was deconvolved for each of the pulses measured above 100 V, normalized to the same total drift time, and averaged. Fig. 2 shows the evaluated function $Q(t)$, along with the response function of the preamplifier $R(t)$. The pulse shapes were then fitted with the single function $Q(t/t_{drift})$, the response function $R(t)$, and t_{drift} as the fitting parameters.

3.2. Electron drift velocities and mobility

The transient current technique (TCT) (see for instance Ref. 7) was used to measure the electron drift velocities in the CZT detectors. We chose the transient signals induced on the central pixels, because of the specific shape of the pixel pulses. The pulse start-time

was determined with high precision by using the laser trigger, while the end of the drift was determined by fitting the fast rising part of the pixel signal. The fitting algorithm, employed to evaluate the functions $Q(t)$ described in the previous section, was also used to estimate the electron drift velocity. To improve accuracy, the induced signal from the adjacent pixel was used to subtract out the slowly rising part of the transient signal read out from the central pixel. The estimated accuracy for measured transient times was about 10 ns. It should be mentioned that the transient current technique works well when the electric field is homogeneous[8]. In high resistive semiconductors with rectifying contacts the space charge creates an electric field gradient[9] that may affect the drift velocity measurements. As a result, the measured electric field strength (the ratio of bias voltage to detector thickness) and drift velocity (the ratio of detector thickness to transient time) are the mean across the CZT sample values. The results of the fitting procedure applied to the signals read out from a selected pixel for different bias are shown in Fig. 3

Fig. 4 shows the typical measured dependence of the drift velocity versus electric field strength for a 450 μm pixel contact. A linear fit gives an estimate of the electron mobility. We found that the mobility varies slightly from pixel to pixel (e.g. the difference in the values measured in the opposite corners of the detector can exceed 15%). The values found for the CZT samples vary between 800 and 900 cm^2/sV (at room temperature, ~21C). These values are smaller than previously reported for the electron mobility, ~1000 cm^2/sV (see Refs. 4 and 10), most likely because of the non-uniformity of the electric field. As seen from Fig. 4, the fit lines intersect the electric field axis at about 0.08 kV/cm (the corresponding voltage shift is ~15 V). This suggests that the electric field is not uniform inside the CZT sample.

3.3. Electron lifetime measurements

For these measurements the laser beam was focused over the center of the pixel contacts. The sum of the induced signal from the cathode and collected signal from the central pixel were measured for several bias voltages. The resulting signal, which resembles the signal from adjacent pixels shown in Fig. 1, contains all the information needed to estimate the electron lifetime. The signal has a maximum corresponding to a time t_{pixel}, when the pixel starts to "see" the approaching electron cloud, and a constant amplitude portion, which is directly proportional to the charge losses due to trapping. The existence of this level is a result of the shielding effect of surrounding pixels i.e. the portion of the charge induced by trapped electrons on the pixel contact is an order of magnitude smaller than on the cathode.

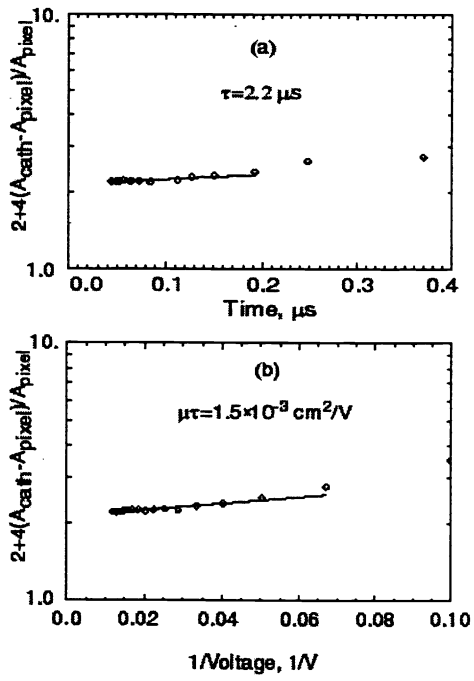

Figure 5. Dependencies $2+4(A_{cath}-A_{pixel})/A_{pixel}$ vs. t_{pixel} *(a)* and $2+4(A_{cath}-A_{pixel})/A_{pixel}$ vs. $1/V$ *(b)* measured for 450 μm contact.

The time t, measured from the beginning of the pulse, could be easily and precisely measured (the starting time of the signal is defined by the laser trigger). We assume as a first approximation, that from this time, the induced charge on the pixel contact increases as a linear function of time from zero up to the maximum value. The amplitude (absolute values) of the signal induced on the cathode A_{cath} and on the pixel A_{pixel} can be written as (normalization coefficient is omitted):

$$A_{cath}=Q_0-KQ_0(1-\exp(-t_{drift}/\tau)) \quad (1)$$

where Q_0 is the original charge generated by the laser pulse at the cathode, t_{drift} is the drift time, τ is the electron lifetime, and K is a coefficient that depends on the spatial distribution of the trapped charge. In the case of uniform distribution (small charge loses) $K=1/2$. Similarly, the charge collected on the pixel contact is:

$$A_{pixel}=Q_0\exp(-t_{drift}/\tau)+KQ(1-\exp(t_{pixel}-t_{drift})/\tau)) \quad (2)$$

where Q is the amount of charge in the cloud at the time t_{pixel}, $KQ(1-\exp(t_{pixel}-t_{drift})/\tau))$ is the charge loses from the time t, until the electron cloud reaches the pixel contact. Thus for the difference of the amplitudes one can write:

$$A_{cath}-A_{pixel}=Q_0(1-\exp(-t/\tau))/2 \quad (3)$$

This equation could be used to estimate the electron lifetime by taking the sum of the cathode and pixel signals and measuring t_{pixel} directly with the digital oscilloscope. Unfortunately, in our case the ionizing source (laser beam) was not sufficiently stable for this measurement. To eliminate this problem we employed a different function: $(A_{cath}-A_{pixel})/A_{pixel}$. If we assume that the charge loss is small and $A_{pixel}=Q_0$, then the first order approximation for τ can be found by fitting the measured dependence, $1+2(A_{cath}-A_{pixel})/A_{pixel}$ versus t with Eq. 3. We then correct τ by putting:

$$A_{pixel}=Q_0 exp(-t_{drift}/\tau) \quad (4)$$

and recalculate a new τ. The dependence of $2(1+2(A_{cath}-A_{pixel})/A_{pixel})$ measured for the 450 μm contacts, and voltages between 100 and 900 V are shown in Fig. 5 (a) (we have multiplied $1+2(A_{cath}-A_{pixel})/A_{pixel}$ by a factor of 2 to shift the curves in the center of the plots). From these and similar dependencies we found that the electron lifetime lies between 2.0 and 2.4 μs for CZT material produced by one vendor, and between 1.6 and 1.9 μs for another supplier. The deviation from the line at low fields is due to charge sharing and non-uniform charge losses. It is noted that for several pixels, we found very low values of τ, having ~0.2-0.5 μs.

The same equation can be used for estimating the $\mu\tau$-product. The only difference is that in this case we do not measure t_{pixel} but the electric field (i.e. voltage V on the cathode). Fig. 5(b) shows a plot of $2(1+2(A_{cath}-A_{pixel})/A_{pixel})$ versus $1/V$ measured for 450μm pixel contacts. The fitting algorithm yields a value of 1.5×10^{-3} cm^2/V for the $\mu\tau$-product.

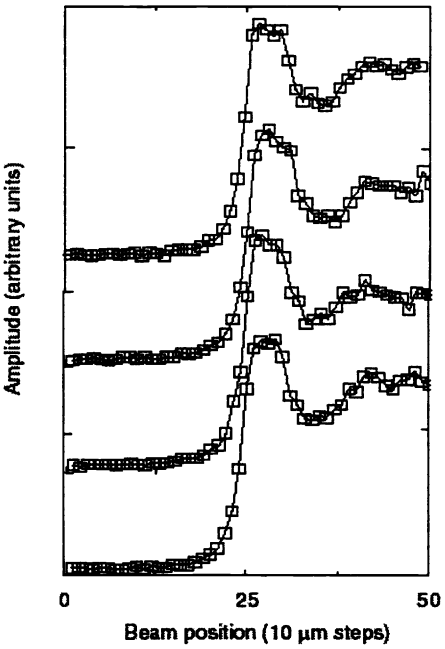

Figure 6. Laser beam scan profiles near the edge.

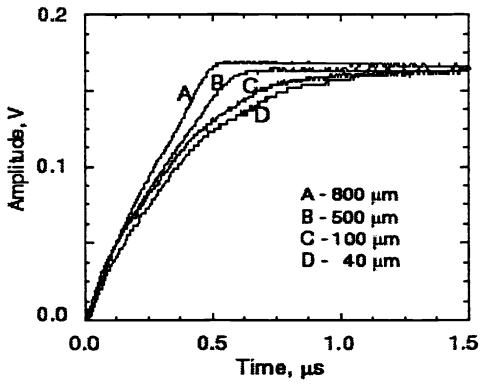

Figure 7. The change in the cathode pulse shape for four edge distances (A-D).

3.4. Studies of edge effect

For the development of actual CZT detectors, it is important to know the width of the dead area near the edges of the CZT detector (the area from which the collection efficiency is significantly degraded). Simple consideration suggests that in the case of a CZT detector with planar contacts extended all the way to the perpendicular edge, the electric field lines are parallel to the side surfaces. For this geometry the electron diffusion process governs the width of the dead area, which can exceed ~100 μm or more. Numerous defects and impurities located at the surface (space charge layer) will trap electrons diffusing toward the side surfaces. However, if one of the electrodes (anode) is placed at some distances from the edge, the field lines beginning on the cathode near the edge will be forced inside the bulk of the CZT material, away from the edges. In this case the width of the dead area will be determined by material uniformity near the edge rather than carrier diffusion.

The detectors used in these measurements had pixel contacts enclosed within a guard ring located 1 mm from the detector edges. The cathode contact covered the whole surface on the opposite side. The laser beam focused on the cathode was moved across the edge of the detector using 10 μm steps, and the signals induced on the cathode were read out with a digital oscilloscope. The results of the scan are shown in Fig. 6, where the signal amplitude is plotted versus beam position. For four scans, as seen, the amplitude of signals drops within ~30 μm from the edge. This value is consistent with the typical penetration depth of cracks formed during CZT dicing. The sharp increase in amplitude near the edge is a result of the non-uniformity of the cathode contact near the edge. Visual inspection under a microscope revealed that the gold contact was not smooth near the edge, and ended approximately 10-50 μm from the true geometric CZT edge. This is indicated in Fig. 6 as a slight decrease in amplitude followed by a sharp increase near the edge

(note that a bare CZT surface reflects less).

As mentioned previously, the field lines originating near the edge are bent away from the side surface of the CZT. Bending of the field lines toward the CZT bulk is illustrated in Fig. 7, which shows the cathode pulse shapes measured at different beam locations near the edge. As seen, the closer the beam position is to the edge, the longer the rise time of the signal. Long pulse rise times implies more field curvature and hence longer trajectories for the collected electrons.

3.5. Scan of CZT pixel detectors

The laser test system was also used to study the pixel response uniformity of CZT pixel detectors. The advantages of using the laser over an X-ray generator, which is typically used for these kinds of measurements, are significantly better collimation and speed. The X-ray beam, say generated by a Mo X-ray tube, can be collimated to a ~50 μm spot size (gaussian beam profile) with a reasonable count rate (~200 events per second) by using the asymmetric Bragg scattering technique[2]. The laser beam can be focused to less than a 10 μm size with a rectangle profile. In the case of X-rays the spectrum must be accumulated for at least several minutes to find the pixel response, while with the laser approach we are employing a signal laser pulse is adequate to evaluate the response.

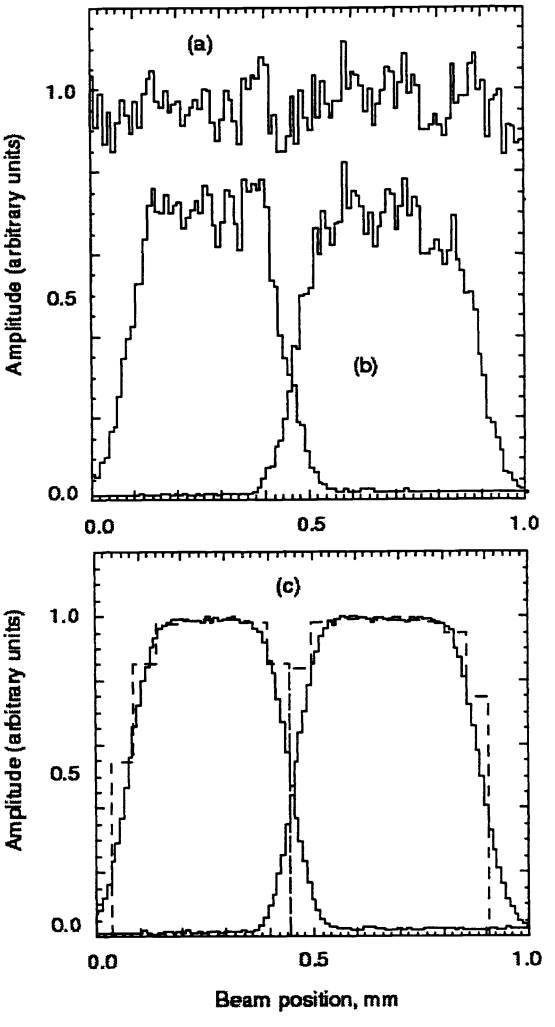

Figure 8. Variation of the pulse-heights from the cathode (a) and two adjacent pixels before (b) and after (c) normalization as the laser beam was scanned from one pixel to the other. The dashed line is the profile measured with X-rays. The contact size is 400 μm, and the gap between the contact is 100 μm.

Two linear actuators controlled by a PC were used to position the detector with respect to the laser beam. The detector response was measured over a two-dimensional geometric grid (beam locations) with a 10 μm pitch. For each beam position, we recorded several (typically 5) events consisting of pulse-heights from four adjacent pixels. To eliminate the fluctuations in the number of excess carriers produced (due to reflection and non-uniformity of the metal contact) we also recorded pulse-heights from the cathode, which were used to normalize the pixel responses to the same charge initially produced near the cathode. These data were used to evaluate the pulse-height profiles, and correlation of pulse-heights from adjacent pixels.

As an example, Fig. 8(a,b) shows the variation of the pulse-heights from adjacent pixels (400 μm contact size; 100 μm inter-pixel gap), and the cathode, as the laser beam was scanned from one pixel to the other. The profiles of normalized pulse-heights are shown in Fig. 8(c). For comparison, the profiles measured for the same two pixels using X-rays (50 μm steps) are also shown. It took ~3 min to measure the profiles shown in Fig. 8 with the laser and ~1 hour with x-rays. Because of the electron diffusion, the signal is shared when the beam is positioned between the pixel contacts. This effect can be seen in Fig. 8 as smoothed profile edges. By fitting the edges we found the electron diffusion coefficient to be ~30 cm^2/s. (The profiles were measured at a bias of -300 V; this corresponds to the 160 ns electron drift time.) For comparison, the Einstein equation for the diffusion coefficient gives 25 cm^2/s.

Fig. 9 shows the correlation of pulse-heights from adjacent pixels. Here the signal amplitude from one pixel is plotted versus the amplitude for the adjacent one as the X-ray beam was scanned across the 100 μm inter-pixel gap. If there is no signal loss the points on this plot should lie on a straight line. As we found in

our previous work[2], for the 450 μm contact case (50 μm gap between contacts) charge splitting occurs between pixels with no signal loss. For the case of the 400 μm contact size (100 μm gap), the results were not clear due to a large electronic noise contribution. The small curvature, which indicates some signal loss, is clearly seen in Fig. 9.

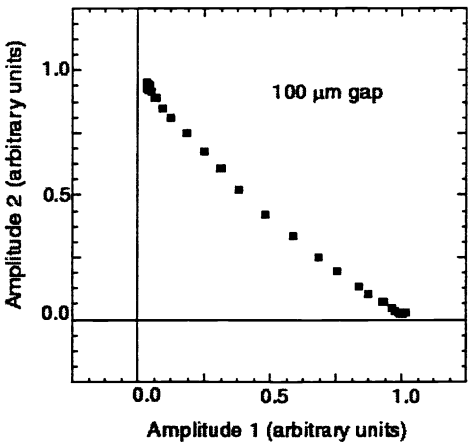

Figure 9. Correlation of pulse-heights from two adjacent pixels. The contact size is 400 μm; the gap between the contacts is 100 μm.

4. CONCLUSION

We have demonstrated using several measurements as examples, that a pulsed laser can be used for testing the performance of CZT detectors, in addition to characterizing detector-grade CZT crystals. The laser approach allows us to estimate the electron lifetime, which was found to be between 1.6 and 2.4 μs for different samples and pixel contact size, and to measure the dependence of the electron drift velocity versus electric field. The estimates for the electron mobility, 700-900 cm^2/sV at ~21C, obtained from these measurements, were (20-30)% less than typically reported values. This suggests that the electric field is non-uniform in the CZT samples used in these measurements. We also studied the edge effects of the CZT detectors with respect to charge collection efficiency for events near the edge. We found that the CZT material does not exhibit any significant signal loss until 20-30 μm from the edge. However, because of diffusion, a significant fraction of the electrons from the cloud produced within ~100 μm from the edge could reach the surface charge layer at the edge, and become trapped. The latter effect can be eliminated if the field lines are bent away from the edge by choosing a proper contact geometry. In this case the detector working area can be extended up to ~30 μm from the edges.

REFERENCES

1 W.W.Craig, F.E. Christensen, T. Decker, C.J. Hailey, F.A. Harrison, R.M. Hill, M. Jimenez-Garate, P. Mao, S. Schindler, SPIE Proc.**3445**, pp.112-120, *EUV, X-Ray, and Gamma-Ray Instrumentation for Astronomy IX*, 1998

2 A. E. Bolotnikov W. R. Cook, F. A. Harrison, A.-S. Wong, S. M. Schindler, A. C. Eichelberger, accepted for publication in Nucl. Instr. And Meth., A (1999).

3 A. Arodzero, J.E. Brau, R.E. Frey, et all., *IEEE Trans. On Nucl. Sc.*, Vol. 43, No. 3, 1180-1187 (1996).

4 K. Suzuki, S. Seto, S. Dairaku, et all., J. Electron. Materi., 25 (1996) 1241-1246.

5 J. E. Toney, B. A. Brunett, T. E. Schlesinger and R. B. James, *IEEE Trans. On Nucl. Sc.,* Vol. 44, No. 4, 1684 (1997).

6 A. J. Syllaios, P.-K. Liao, B. J. Greene, et all., J. Electron. Materi., 26 (1997) 567-570.

7 LightPath Technologies, Inc.

8 V. Eremin and Z. Li, Nucl. Instr. And Meth., A362 (1995) 338-343.

9 C. Manfredotti, F. Fizzotti, P. Polesello et all., Nucl. Instr. And Meth., A380 (1996) 136-140.

10 K. Parnham, Nucl. Instr. And Meth., A377 (1996) 487-491.